JOC*Article*

CASPT2//CASSCF Study on the Photolysis Mechanism of 2,3-Diazabicyclo[2.1.1]hex-2-ene: α C−N versus β C−C Cleavage

Hui Chen and Shuhua Li*

School of Chemistry and Chemical Engineering, Institute of Theoretical and Computational Chemistry, Lab of Mesoscopic Chemistry, Nanjing University, Nanjing, 210093, P. R. China

shuhua@nju.edu.cn

Received June 7, 2006

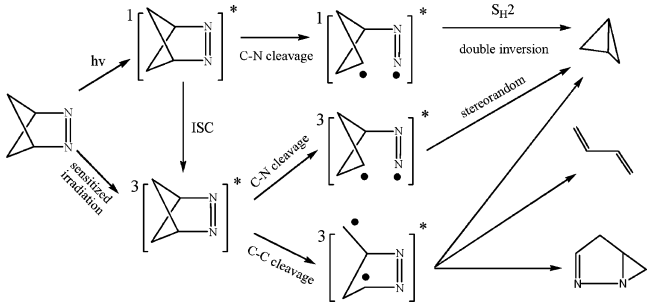

A CASPT2//CASSCF study has been carried out to investigate the mechanism of the photolysis of 2,3-diazabicyclo[2.1.1]hex-2-ene under direct irradiation and triplet-sensitized irradiation. By exploring the detailed potential energy surfaces and surface crossing points for several low-lying excited states, we have been able to provide a tentative description on the photophysical and photochemical processes of this compound. According to our calculations, on the S_1 surface one C−N bond is broken first to generate the diazenyl biradicals, which then result in the photoproduct bicyclobutane through a concerted C−N cleavage and C−C coupling process. The intersystem crossing (ISC) from the S_1 state to the triplet state was found to be quite efficient, which could account for two other photoproducts (butadiene and 1,2-diazabicyclo[3.1.0]hex-2-ene) on direct irradiation. On the T_1 surface, the C−C bond cleavage could readily take place to generate the triplet hydrazonyl biradical. One deactivation path of this intermediate is to convert into the corresponding singlet biradical by an ISC process. Then this biradical undergoes a barrierless C−N bond formation to form the photoproduct 1,2-diazabicyclo[3.1.0]hex-2-ene. Another path of the triplet hydrazonyl biradical is to form the intermediate 2-allyl-diazomethane through a C−N cleavage. This intermediate will break another C−N bond to produce a terminal carbene species, which is easily converted into butadiene and bicyclobutane by 1,2-hydrogen shift reaction and addition to C═C double bond, respectively.

1. Introduction

Azoalkanes have attracted much attention due to their potential utility in organic synthesis of structurally unusual compounds.[1−7] Among the series of homologous bridged bicyclic azoalkanes, 2,3-diazabicyclo[2.1.1]hex-2-ene (**1**), which is the smallest and most strained member, displayed a very complex photochemical behavior that is quite different from that in its higher homologues, 2,3-diazabicyclo[2.2.1]hep-2-ene (DBH)[8−20] and 2,3-diazabicyclo[2.2.2]oct-2-ene (DBO).[21−34]

(1) Engel, P. S. *Chem. Rev.* **1980**, *80*, 99.
(2) Rau, H. *Angew. Chem., Int. Ed. Engl.* **1973**, *12*, 224.
(3) Meier, H.; Zeller, K. P. *Angew. Chem., Int. Ed. Engl.* **1977**, *16*, 835.
(4) Adam, W.; De Lucchi, O. *Angew. Chem., Int. Ed. Engl.* **1980**, *19*, 762.
(5) Adam, W.; Grabowski, S.; Wilson, R. M. *Acc. Chem. Res.* **1990**, *23*, 165.
(6) Dougherty, D. A. *Acc. Chem. Res.* **1991**, *24*, 88.
(7) Engel, P. S.; Hayes, R. A.; Kiefer, L.; Szilagyi, S.; Timberlake, J. W. *J. Am. Chem. Soc.* **1978**, *100*, 1876.
(8) Solomon, B. S.; Thomas, T. F.; Steel, C. *J. Am. Chem. Soc.* **1968**, *90*, 2249.
(9) Roth, W. R.; Martin, M. *Justus Liebigs Ann. Chem.* **1967**, *702*, 1.
(10) Engel, P. S. *J. Am. Chem. Soc.* **1969**, *91*, 6903.
(11) Allred, E. L.; Smith, R. L. *J. Am. Chem. Soc.* **1969**, *91*, 6766.
(12) Adam, W.; Oppenlander, T.; Zang, G. *J. Org. Chem.* **1985**, *50*, 3303.
(13) Adam, J. S.; Weisman, R. B.; Engel, P. S. *J. Am. Chem. Soc.* **1990**, *112*, 9115.

10.1021/jo0611622 CCC: $33.50
Published on Web 11/01/2006

SCHEME 1

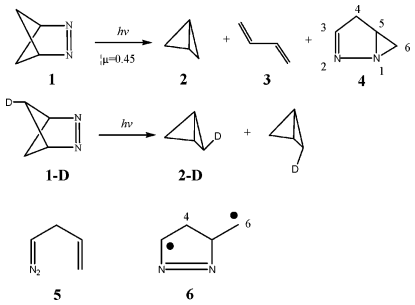

Azoalkane **1** was first synthesized by Dougherty et al.[35] The UV spectrum of **1** is highly structured with the 0−0 excitation band at 331 nm (86.4 kcal/mol). Fluorescence was observed for **1** with $\lambda_{max} = 337$ nm (84.8 kcal/mol) in hexane. As shown in Scheme 1, photolysis of **1** in benzene or cyclohexane produces bicyclo[1.1.0]butane (**2**), butadiene (**3**), and 1,2-diazabicyclo-[3.1.0]hex-2-ene (**4**).[34] The quantum yield for overall decomposition of **1** upon direct photolysis at 298 K was measured to be 0.45 ± 0.05. Nevertheless, the relative yields were found to sensitively depend on temperature and spin multiplicity. On direct irradiation at 298 K, **2** is the dominant product. While on triplet-sensitized irradiation or direct irradiation at lower temperature (173 K), **4** is the major product.

The photolysis of *exo*-5-^{2}H-**1** (**1-D**) gives a 47% excess of the double-inversion product, *exo*-2-^{2}H-**2** (**2-D**), as shown in Scheme 1.[34] This situation is similar to the photolysis of exo-deuterated DBH (DBH-d_2) where a 20% excess of inversion was observed.[9] However, in the solution phase, thermolysis of **1-D** produces stereorandomized **2-D**.[36]

Among the photolysis products, the formation of hydrazone **4** is unusual in the photolysis of the bicyclic azoalkanes because this type of photoproduct was not observed in DBH and DBO but was only seen in a few DBH derivatives.[15−17] Both direct and sensitized photolysis of **1-D** produced **4** with completely stereospecific labeling at the C4 atom but complete scrambling at the C6 atom.[34] This result demonstrated an irreversible β C−C cleavage to produce a stereorandom hydrazonyl biradical (**6**). Concerning the other products **2** and **3**, the experiments showed that 2-allyldiazomethane (**5**)[34] is the precursor to both **2** and **3** in the triplet manifold. Several pieces of evidence suggested that the intersystem crossing (ISC) from the lowest singlet excited-state to the triplet state in **1** is fairly efficient, unlike that in its related DBH and DBO systems.[34]

Although the experimental results have answered some problems on the photolysis mechanism of **1**, there are still many important questions to be answered. For example, is the ISC of **1** from the singlet excited state to the triplet excited state really efficient? What is the mechanism of the generation of the intermediate **5** from **1**? How to understand the preferred double-inversion product **2-D** during the photolysis? In this paper we will perform a detailed theoretical study on the photolysis mechanism of **1**, which is aimed to understand all the questions mentioned above. By using the CASPT2//CASSCF method we will investigate the energies and structures of various stationary points and crossing points on the potential energy surfaces (PESs) of several low-lying excited states (S_1, T_1, T_2) possibly involved in the photolysis of **1**. On the basis of these information, we will give detailed discussions on possible reaction paths involved in the photolysis mechanism of **1**.

2. Computational Details

The CASSCF[37] geometry optimizations for ground-state and excited-state stationary points, conical intersections (CI) and singlet−triplet crossing points were carried out using the MCSCF program distributed in Gaussian03 package[38] with a 6-311G** basis. For each stationary point on the PES, a frequency calculation was performed to obtain its zero-point energy (ZPE) and to verify whether it is a minimum or a transition state. Geometry optimizations of the surface crossing points were performed with the state-averaged CASSCF method. To include dynamic correlation energies, single-point internally contracted CASPT2[39,40] calculations with the same basis set, the active spaces (and the same weights for state-averaged calculations) were carried out with the Mol-

(14) Simpson, C. J. S. M.; Wilson, G. J.; Adam, W. *J. Am. Chem. Soc.* **1991**, *113*, 4728.
(15) Adam, W.; Nau, W. M.; Sendelbach, J.; Wirtz, J. *J. Am. Chem. Soc.* **1993**, *115*, 12571.
(16) Adam, W.; Nau, W. M.; Sendelbach, J. *J. Am. Chem. Soc.* **1994**, *116*, 7049.
(17) Adam, W.; Fragale, G.; Klapstein, D.; Nau, W. M.; Wirtz, J. *J. Am. Chem. Soc.* **1995**, *117*, 12578.
(18) Sherill, C. D.; Seidl, E. T.; Schaefer, H. F., III. *J. Phys. Chem.* **1992**, *96*, 3712.
(19) Yamamoto, N.; Olivucci, M.; Celani, P.; Bermardi, F.; Robb, M. A. *J. Am. Chem. Soc.* **1998**, *120*, 2391.
(20) Sinicropi, A.; Page, C. S.; Adam, W.; Olivucci, M. *J. Am. Chem. Soc.* **2003**, *125*, 10947.
(21) Clark, W. D. K.; Steel, C. *J. Am. Chem. Soc.* **1971**, *93*, 6347.
(22) Engel, P. S.; Steel, C. *Acc. Chem. Res.* **1973**, *6*, 275.
(23) Engel, P. S.; Nalepa, C. J. *Pure Appl. Chem.* **1980**, *52*, 2621.
(24) Engel, P. S.; Horsey, D. W.; Key, D. E.; Nalepa, C. J.; Soltero, L. R. *J. Am. Chem. Soc.* **1983**, *105*, 7108.
(25) Engel, P. S.; Keys, D. E.; Kitamura, A. *J. Am. Chem. Soc.* **1985**, *107*, 4964.
(26) Edmunds, A. J. F.; Samuel, C. J. *J. Chem. Soc., Perkin Trans.* 2 **1989**, 1267.
(27) Anderson, M. A.; Grissom, C. B. *J. Am. Chem. Soc.* **1995**, *117*, 5041.
(28) Anderson, M. A.; Grissom, C. B. *J. Am. Chem. Soc.* **1996**, *118*, 9552.
(29) Caldwell, R. A.; Helms, A. M.; Engel, P. S.; Wu, A. *J. Phys. Chem.* **1996**, *100*, 17716.
(30) Roberson, M. J.; Simons, J. *J. Phys. Chem. A* **1997**, *101*, 2379.
(31) Nau, W. M.; Greiner, G.; Wall, J.; Rau, H.; Olivucci, M.; Robb, M. A. *Angew. Chem., Int. Ed.* **1998**, *37*, 98.
(32) Khong, K. S.; Houk, K. N. *J. Am. Chem. Soc.* **2003**, *125*, 14867.
(33) Chen, H.; Li, S. H. *J. Am. Chem. Soc.* **2005**, *127*, 13190.
(34) Chang, M. H.; Dougherty, D. A. *J. Org. Chem.* **1981**, *46*, 4092. See also: Amey, R. L.; Smart, B. E. *J. Org. Chem.* **1981**, *46*, 4090.
(35) Chang, M. H.; Dougherty, D. A. *J. Am. Chem. Soc.* **1982**, *104*, 2333.
(36) Chang, M. H.; Dougherty, D. A. *J. Am. Chem. Soc.* **1982**, *104*, 1131.
(37) Roos, B. O. *Adv. Chem. Phys.* **1987**, *69*, 399.
(38) Frisch, M. J.; Trucks, G. W.; Schlegel, H. B.; Scuseria, G. E.; Robb, M. A.; Cheeseman, J. R.; Montgomery, J. A., Jr.; T. V.; Kudin, K. N.; Burant, J. C.; Millam, J. M.; Iyengar, S. S.; Tomasi, J.; Barone, V.; Mennucci, B.; Cossi, M.; Scalmani, G.; Rega, N.; Petersson, G. A.; Nakatsuji, H.; Hada, M.; Ehara, M.; Toyota, K.; Fukuda, R.; Hasegawa, J.; Ishida, M.; Nakajima, T.; Honda, Y.; Kitao, O.; Nakai, H.; Klene, M.; Li, X.; Knox, J. E.; Hratchian, H. P.; Cross, J. B.; Adamo, C.; Jaramillo, J.; Gomperts, R.; Stratmann, R. E.; Yazyev, O.; Austin, A. J.; Cammi, R.; Pomelli, C.; Ochterski, J. W.; Ayala, P. Y.; Morokuma, K.; Voth, G. A.; Salvador, P.; Dannenberg, J. J.; Zakrzewski, G.; Dapprich, S.; Daniels, A. D.; Strain, M. C.; Farkas, O.; Malick, D. K.; Rabuck, A. D.; Raghavachari, K.; Foresman, J. B.; Ortiz, J. V.; Cui, Q.; Baboul, A. G.; Clifford, S.; Cioslowski, J.; Stefanov, B. B.; Liu, G.; Liashenko, A.; Piskorz, P.; Komaromi, I.; Martin, R. L.; Fox, D. J.; Keith, T.; Al-Laham, M. A.; Peng, C. Y.; Nanayakkara, A.; Challacombe, M.; Gill, P. M. W.; Johnson, B.; Chen, W.; Wong, M. W.; Gonzalez, C.; Pople, J. A. *Gaussian 03*, Revision B.04; Gaussian, Inc., Pittsburgh PA, 2003.
(39) Werner, H. J. *Mol. Phys.* **1996**, *89*, 645.
(40) Celani, P.; Werner, H. J. *J. Chem. Phys.* **2000**, *112*, 5546.

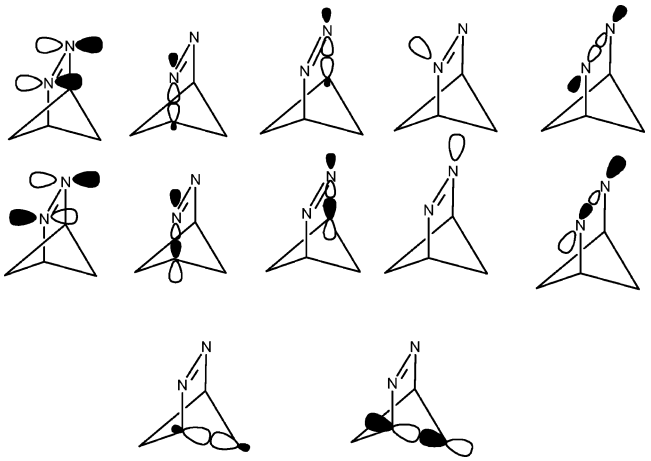

FIGURE 1. Active space used in our CASSCF calculations.

pro2000 package[41] at the CASSCF-optimized geometries. A level shift of 0.2 was used in all CASPT2 calculations to avoid intruder state problems.[42] Spin−orbit coupling constants were calculated using the full Breit-Pauli SO operator[43] with the Molpro2000 package. To determine the reaction paths on a given excited-state surface, we have done intrinsic reaction coordinate (IRC) calculations. Approximate minimum energy path (MEP) calculations have been used to build the connection between the stationary points and the conical intersections or singlet−triplet crossing points (exact MEP calculations are still difficult for systems as large as **1**).

The active spaces used in our CASSCF and CASPT2 calculations are shown in Figure 1. To describe the cleavage of two C−N bonds, we employed an active space (12,10) which includes both pairs of C−N σ and σ^* orbitals and six orbitals from the N_2 fragment (π, π^*, two n orbitals, and σ, σ^*), as shown in Figure 1. In regions near the diazenyl biradicals of the PES, the lone pair orbital of the nitrogen atom of the broken C−N bond is nearly doubly occupied in all states under study. To ensure the convergence of the CASSCF calculations, we remove this orbital from the active space to form a (10,9) active space. It should be mentioned that the CASPT2 energies obtained with two slightly different active spaces can be approximately compared.[33] To study the β C−C cleavage process, we modified the active space (12,10) described above as follows. First, we add a pair of C−C σ and σ^* orbitals. Then, one n orbital of the nitrogen atom, which is nearly doubly occupied in all states under study, is placed in the inactive space. The resulting active space, (12,11), was used to explore the triplet state PES of the β C−C cleavage and the subsequent processes. To study the PES of allyl-methylene without the N_2 fragment, the active space consists of a pair of C=C π and π^* orbitals, two p orbitals at the carbene C atom, and the corresponding C−H σ and σ^* orbitals if a hydrogen atom transfer process is concerned.

It is important to estimate the accuracy of the method and the basis set we used in this work. With the CASPT2//CASSCF method and the 6-311G** basis set, the calculated singlet 0−0 energy gap of **1** is 85.4 kcal/mol (ZPE corrections calculated at the CASSCF/6-311G* level are added) with an active space (12,10). This value agrees well with the corresponding experimental value of 86.4 kcal/mol[35] in *n*-hexane. In addition, with the same active space the vertical emission energy (from the excited singlet state at its equilibrium geometry) is calculated to be 85.6 kcal/mol at the CASPT2 level, being also close to the measured fluorescence maximum of **1** (84.8 kcal/mol). Our calculations here and results from others for similar systems[19,20,31−33] demonstrate that the CASPT2//CASSCF method with the 6-311G** basis set could give reliable descriptions of ground-state and excited-state PESs of **1**.

3. Results and Discussion

In this section, we will present our results into four subsections. The first one includes the PESs of S_0, S_1, T_1, and T_2 near the ground-state equilibrium geometry of **1**. Then, the decay pathways from the excited singlet and triplet states are discussed, respectively. In the second subsection, we will describe the PESs of the low-lying excited states in the C−N breaking region and in the vicinity of the diazenyl biradicals, and discuss possible reaction paths for production of bicyclobutane. Excited-state PESs and possible reaction paths involving the β C−C bond cleavage will be described in the third subsection. In the final subsection, we will make a comparison of our results for **1** with the previous theoretical results for related DBH and DBO.

3.1. The Excited State PESs near the Ground-State Equilibrium Geometry. 3.1.1. Stationary Points. For all stationary points and crossing points near the ground-state equilibrium geometry, their optimized geometries from CASSCF(12,10) calculations are shown in Figure 2, and their energies are listed in Table 1. As shown in Figure 2, the ground-state minimum M_1−S_0 of **1** is of C_{2v} symmetry with the N−N bond and C−N bond lengths being 1.260 and 1.551 Å, respectively. Single-point CASPT2 calculations show that the vertical excitation energies for S_0−T_1, S_0−S_1, and S_0−T_2 are 69.7, 87.0, and 105.9 kcal/mol, respectively, as shown in Table 1. Thus, on triplet-sensitized irradiation with benzene (E_T = 84.7 kcal/mol) as a triplet sensitizer, only the T_1 state is accessible. In the Franck−Condon region of the S_1 (n−π^*) surface, we located a minimum (M_1−S_1) of C_{2v} symmetry with r(N−N) = 1.291 Å. Interestingly, in related systems DBO and DBH the corresponding symmetric stationary points on the S_1 surface are all transition states whose imaginary vibrational modes correspond to the twisting[33] and the bending[19] of the C−N=N−C bridge, respectively. A comparison of these results indicates that **1** is more strained than DBH and DBO. The calculated singlet (0−0) energy gap is 85.4 kcal/mol with ZPE corrections (87.4 without ZPE corrections) at the CASPT2 level, which agrees well with the experimental result of 86.4 kcal/mol. We notice that the calculated 0−0 energy gap is slightly larger than the vertical excitation energy at the CASPT2 level. This unphysical situation is due to the fact that the minimum structure obtained at the CASSCF level is different from the true minimum at the CASPT2 level (which is not available at the present time). The vertical emission energy from M_1−S_1, calculated to be 85.6 kcal/mol at the CASPT2 level, is also in good agreement with the fluorescence maximum of **1** (84.8 kcal/mol).

Now let us turn to the triplet states. On the PESs of the lowest two triplet states, T_1 (n−π^*) and T_2 (π−π^*), we located two transition states, TS_1−T_1 and TS_2−T_1 of C_{2v} symmetry. The imaginary vibrational modes in both of these two transition states correspond to the twisting of the C−N=N−C bridge. TS_1−T_1 is 0.8 kcal/mol lower in energy than TS_2−T_1 at the CASPT2 level. The main geometrical difference of these two transition states is that the N−N bond length is much longer in TS_2−T_1 (1.577 Å) than that in TS_1−T_1 (1.282 Å). Interestingly, the

(41) Amos, R. D.; Bernhardsson, A.; Berning, A.; Celani, P.; Cooper, D. L.; Deegan, M. J. O.; Dobbyn, A. J.; Eckert, F.; Hampel, C.; Hetzer, G.; Knowles, P. J.; Korona, T.; Lindh, R.; Lloyd, A. W.; McNicholas, S. J.; Manby, F. R.; Meyer, W.; Mura, M. E.; Nicklass, A.; Palmieri, P.; Pitzer, R.; Rauhut, G.; Schütz, M.; Schumann, U.; Stoll, H.; Stone, A. J.; Tarroni, R.; Thorsteinsson, T.; Werner, H.-J. MOLPRO, a package of *ab initio* programs written by H. J. Werner, P. J. Knowles, Version 2000.1; University of Birmingham: UK, 1999.

(42) Roos, B. O.; Andersson, K. *Chem. Phys. Lett.* **1995**, *245*, 215.

(43) Berning, A.; Schweizer, M.; Werner, H. J.; Knowles, P. J.; Palmieri, P. *Mol. Phys.* **2000**, *98*, 1823.

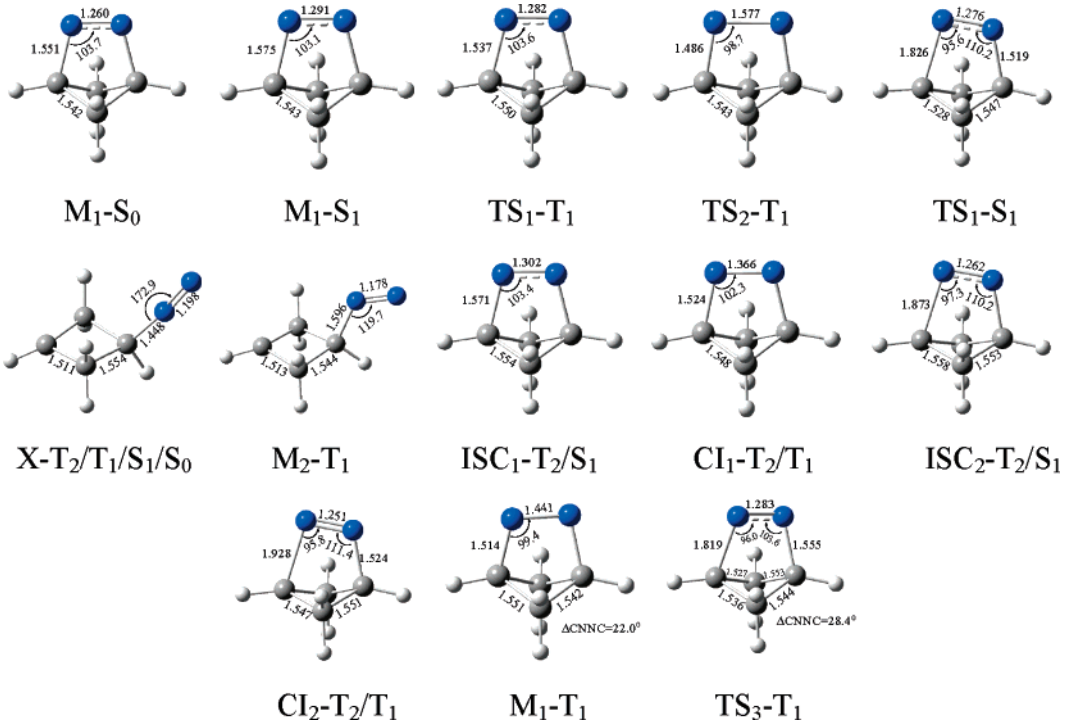

FIGURE 2. CASSCF(12,10)-optimized geometries of minima, transition states, and surface crossing points.

TABLE 1. Calculated CASSCF (12,10) and CASPT2 Energies of Stationary Points and Crossing Points on the Low-Lying Surfaces of 1

		relative energy[a] (kcal/mol)	
geometry	state	CASSCF	CASPT2
M_1-S_0	S_0	0.0	0.0
	T_1 (n−π*)	90.4	69.7
	T_2 ($\pi-\pi$*)	118.5	105.9
	S_1 (n−π*)	106.6	87.0
M_1-S_1	S_1 (n−π*)	105.7	87.4 (85.4)
TS_1-T_1	T_1 (n−π*)	87.8	68.1 (66.4)
TS_2-T_1	T_1 ($\pi-\pi$*)	78.9	69.2 (67.2)
TS_1-S_1	S_1 (n−π*)	107.2	93.0 (90.4)
$X-T_2/T_1/S_1/S_0$[b]	S_0	66.4	67.6
	S_1 (n−π*)	67.0	68.1
	T_1 (n−π*)	66.8	68.1
	T_2 (n−σ*)	66.8	68.5
M_2-T_1(exo)[b]	T_1	29.6	40.0 (34.8)
ISC_1-T_2/S_1[c]	S_1 (n−π*)	108.1	88.2
	T_2 ($\pi-\pi$*)	108.1	97.0
CI_1-T_2/T_1[d]	T_2 ($\pi-\pi$*)	93.7	79.6
	T_1 (n−π*)	93.7	77.2
ISC_2-T_2/S_1[c]	S_1 (n−π*)	114.8	97.0
	T_2 (n−σ*)	114.8	105.2
CI_2-T_2/T_1[d]	T_1 (n−π*)	103.2	85.0
	T_2 (n−σ*)	103.2	95.2
M_1-T_1	T_1 (n−π*−$\pi-\pi$*)	77.8	65.8 (64.2)
TS_3-T_1	T_1	85.2	73.8 (70.8)

[a] The ZPE-corrected energies are shown in parentheses; the energy of the S_0-state energy at M_1-S_0 is set to zero. [b] The structures are optimized at the CASSCF(10,9) level. [c] State-averaged calculation with two states (T_2, S_1) being equally weighted. [d] State-averaged calculation with two states (T_2, T_1) being equally weighted.

energy order of the ^{3}n−π* and $^3\pi-\pi$* states is reversed when the geometry of the molecule changes from TS_1-T_1 to TS_2-T_1. At the geometry of TS_1-T_1 the ^{3}n−π* state lies 30.8 kcal/mol below the $^3\pi-\pi$* state at the CASPT2 level, whereas at the geometry of TS_2-T_1 it lies 30.4 kcal/mol above the $^3\pi-\pi$* state. By following the imaginary vibrational modes of these

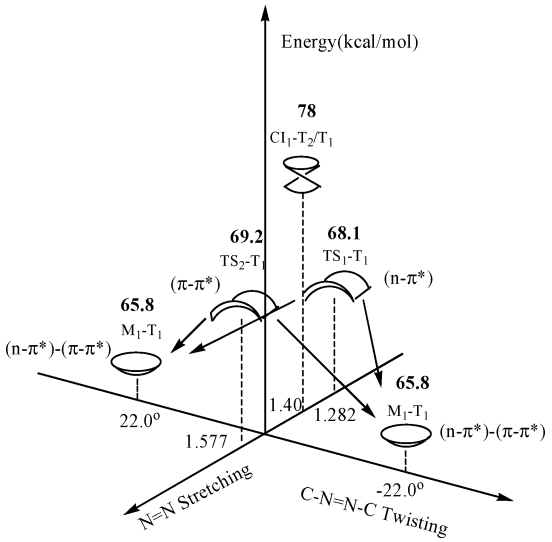

FIGURE 3. Triplet-state PESs near the Franck−Condon region.

two transition states, we obtained the same minimum M_1-T_1 and its enantiomer, of mixed (n−π*)−($\pi-\pi$*) character, as shown in Figure 3. M_1-T_1 is 2.3 kcal/mol lower in energy than TS_1-T_1 at the CASPT2 level and the C−N=N−C twisting angle in M_1-T_1 is 22.0°. Previous studies showed that the corresponding angle is about 30° and 45.7° in the T_1 minimum of DBH[19] and DBO,[33] respectively. Clearly, this difference indicates that **1** is more rigid than DBH and DBO.

From the results described above, one can see that in the Franck−Condon region the T_1 (n−π*) surface exhibits the characteristic of a transition state, while the S_1 (n−π*) surface corresponds to a minimum structure. As a result, on direct irradiation **1** will possibly reach the (n−π*) minimum M_1-S_1, while on triplet-sensitized excitation to T_1 **1** will possibly relax to the twisted minimum M_1-T_1.

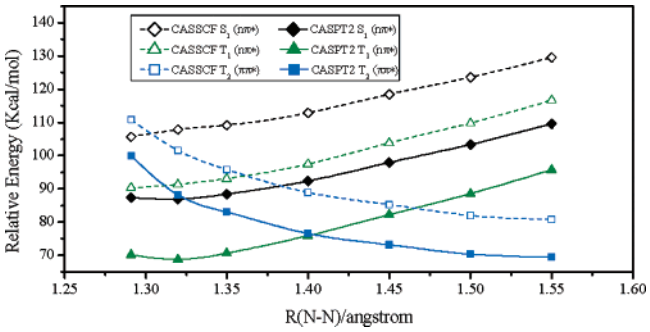

FIGURE 4. CASSCF and CASPT2 energies of the T_1 (n−π*), T_2 (π−π*) and S_1 (n−π*) states as a function of the N−N bond distance.

3.1.2. Crossing Points. Now we will discuss the structures of conical intersections and singlet−triplet crossing points near the S_0 equilibrium geometry. First, our state-averaged CASSCF-(12,10) optimization resulted in a T_2 (π−π*)/S_1 (n−π*) crossing point, ISC_1−T_2/S_1, which is 2.4 kcal/mol above the S_1 minimum M_1−S_1 at the CASSCF level. The geometry of ISC_1−T_2/S_1 is of C_{2v} symmetry with r(N−N) = 1.302 Å, being close to that of M_1−S_1 (1.291 Å). Second, our optimization led to a CI between the T_2 (π−π*) and T_1 (n−π*) states, labeled CI_1−T_2/T_1, being 14.4 kcal/mol lower in energy than ISC_1−T_2/S_1 at the CASSCF level. CI_1−T_2/T_1 is also of C_{2v} symmetry but has a N−N bond length of 1.366 Å, which is a little longer than 1.302 Å in ISC_1−T_2/S_1.

It should be noticed that the near-degeneracy of the T_2 and S_1 states at ISC_1−T_2/S_1 (and that of the T_2 and T_1 states at CI_1−T_2/T_1) obtained at the CASSCF level might be lifted at the CASPT2 level. To estimate the effect of dynamic correlation, we employed an approximate approach, as discussed below (the direct use of the CASPT2 method to optimize the structures of crossing points is not feasible yet for systems as large as **1**). Since the relative energies of the T_1 (n−π*), T_2 (π−π*), and S_1 (n−π*) states are mainly affected by the N−N bond length, we carried out a series of constrained CASSCF optimizations by fixing the N−N bond length at different values, and then performed single-point CASPT2 calculations to correct the energetics. The results are shown in Figure 4. One can see that at the CASPT2 level the T_2/S_1 intersystem crossing is predicted to occur at r(N−N) = 1.33 Å, and the conical intersection (T_2/T_1) is predicted to take place at r(N−N) = 1.40 Å. Correspondingly, the energies of ISC_1−T_2/S_1 and CI_1−T_2/T_1 are about 87 and 78 kcal/mol at the CASPT2 level, respectively, above the ground-state minimum.

3.1.3. Possible Decay Pathways of the Lowest Singlet Excited State. By comparing the structures of M_1−S_1, ISC_1−T_2/S_1, and CI_1−T_2/T_1, we find that upon stretching the N−N bond length M_1−S_1 can reach ISC_1−T_2/S_1 first and then to CI_1−T_2/T_1. Our calculations show that the gradients of the T_2 and S_1 states at ISC_1−T_2/S_1 mainly involve the N−N stretching coordinate. In fact, along the N−N stretching coordinate, the energy profile from M_1−S_1 to ISC_1-T_2/S_1 and to CI_1-T_2/T_1 is already shown in Figure 4. It can be seen from Figure 4 that at the CASPT2 level the system decreases in energy monotonously from M_1−S_1 to ISC_1−T_2/S_1 and to CI_1−T_2/T_1 (remember that the energy of the S_1 minimum M_1−S_1 is 87.4 kcal/mol). In addition, the spin−orbit coupling (SOC) constant between two crossing states is calculated to be 9.4 cm^{-1} at ISC_1−T_2/S_1. Thus, the intersystem crossing from S_1 to T_2 in **1** should be quite efficient due to a barrierless access from M_1−S_1 to ISC_1−T_2/S_1 and a relative large SOC constant between two crossing states. To conclude, it is likely that upon direct excitation the S_1 (n-π*) state relaxes first to ISC_1−T_2/S_1, and then reaches the T_2 (π−π*) state through the intersystem crossing, and finally decays to the T_1 surface through the internal conversion from T_2 (π−π*) to T_1 (n−π*) at CI_1−T_2/T_1.

It should be pointed out that two vibrational modes are important in the excited-state evolution of **1**, as in the DBO system.[33] These two modes are the N═N stretching and the C−N═N−C twisting. The former is responsible for the crossing between the "pure" (n−π*) and (π−π*) states, and the latter causes these two states to mix.

3.2. Excited-State PESs and Reaction Paths Involved in the Production of Bicyclobutane. 3.2.1. Stationary Points and Crossing Points in the C−N Breaking Region. On the S_1 surface, we located an asynchronous C−N bond-breaking transition state, labeled TS_1−S_1. The breaking C−N bond distance is 1.826 Å in TS_1−S_1. At the CASPT2 level, the calculated barrier for this C−N cleavage is 5.0 kcal/mol with ZPE corrections (5.6 kcal/mol without ZPE corrections). This barrier height is comparable to that in DBH (5.7 kcal/mol without ZPE corrections),[20] but significantly lower than that in DBO (10.9 kcal/mol with ZPE corrections).[33] On the T_1 surface, we also found a C−N bond-breaking transition state TS_3−T_1. The breaking C−N bond distance is 1.819 Å in TS_3-T_1, slightly shorter than that in TS_1−S_1. At the CASPT2 level, the activation energy required from M_1−T_1 to TS_3−T_1 is 6.6 kcal/mol with ZPE corrections included (8.0 kcal/mol without ZPE corrections).

In this region, we located a crossing point between the T_2 (n−σ*) and S_1 (n−π*) states (ISC_2−T_2/S_1), and a CI between the T_2 (n−σ*) and T_1 (n−π*) states (CI_2−T_2/T_1). Both structures of ISC_2−T_2/S_1 and CI_2−T_2/T_1 are of C_s symmetry (the C−N═N−C bridge is not twisted) and have a long C−N bond length, 1.873, and 1.928 Å, respectively. The ^{3}n−σ* state is high in energy near the Franck−Condon region, but as the C−N bond is stretched its energy decreases dramatically and eventually it becomes the lowest triplet state. The situation here is similar to that in DBO.[33]

In addition, we located an approximate 4-fold crossing point of T_1, T_2, S_0, and S_1, denoted as X−$T_2/T_1/S_1/S_0$. The structure of this point was determined by performing two geometry optimizations for conical intersections of S_0/S_1 and T_1/T_2, in which an active space (10,9) was used.[44] Since the resulting two conical intersections are structurally very close to each other, the corresponding structure could be viewed as an approximate 4-fold crossing point. As shown in Figure 2, the structure of X−$T_2/T_1/S_1/S_0$ is characterized by a nearly linear N═N−C fragment (∠NNC = 172.9°) and a nearly coplanar arrangement of four carbon atoms. This 4-fold crossing point is structurally very similar to the 4-fold crossing points obtained previously for DBH[19] and DBO.[33] The electron configurations of the four relevant states within the active space at X−$T_2/T_1/S_1/S_0$ are also similar to those in DBO,[33] and thus will not be discussed here. As shown previously for DBO,[33] it should also be a strongly exoergic process for the system **1** to expand the NNC angle to reach the diazenyl biradical region. At the geometry of X−T_2/$T_1/S_1/S_0$, the SOC value between the singlet and triplet surfaces with different electronic configurations is calculated to be 38.3

(44) The (10,9) active space is obtained from the (12,10) active space described in the text by removing the doubly occupied lone pair orbital of the N atom of the broken C−N bond.

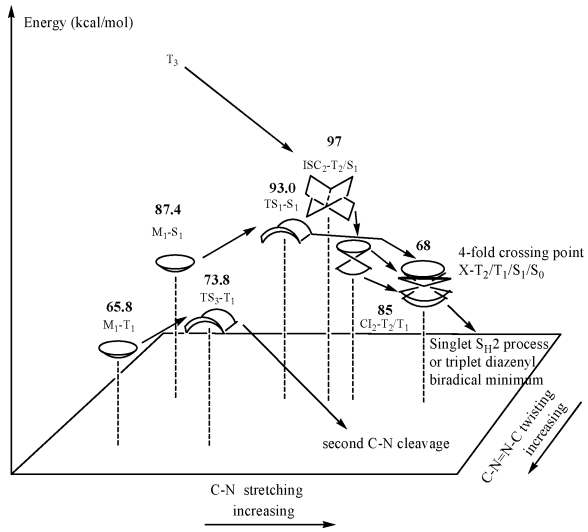

FIGURE 5. Excited-state PESs in the C−N bond-breaking region.

cm^{-1} for S_0 and T_1 and 38.2 cm^{-1} for S_1 and T_2, while the SOC value between surfaces of the same electronic configuration is significantly smaller (2.7 cm^{-1} for S_0 and T_2, and 0.4 cm^{-1} for S_1 and T_1). Thus, our calculations imply that the ISC between the singlet and triplet surfaces with different electronic configurations is likely to occur. On the other hand, since the internal conversion via the conical intersection is fully efficient, the molecule can decay directly from the S_1 surface to the S_0 surface through X−T_2/T_1/S_1/S_0, leading to the S_0 diazenyl biradicals. To summarize, the excited-state PESs in the C−N bond-breaking region are presented in Figure 5.

3.2.2. Excited-State PESs in the Diazenyl Biradical Region. As discussed above, at the 4-fold crossing point it is very likely for the S_1 state to relax to the S_0 surface or the T_1 surface to form singlet or triplet diazenyl biradicals, respectively. However, on the S_0 surface, in spite of numerous attempts, we could not locate any singlet diazenyl biradical minimum with CASSCF(10,9)[44] calculations or CASSCF(4,4)[45] calculations (our geometry optimizations always result in the species bicyclobutane **2**). But, on the T_1 surface, we found a diazenyl biradical minimum M_2−T_1 of the *exo* conformer by performing CASSCF(10,9) calculations.[44] Similar calculations demonstrated that the triplet diazenyl biradicals with *endo* conformers are not minima.

3.2.3. Possible Reaction Paths for Production of Bicyclobutane. On the basis of the excited-state PESs described above, we first discuss the reaction path on the S_1 surface. The calculated ZPE-corrected barrier for breaking the first C−N bond (from M_1−S_1 to TS_1−S_1) is 5.0 kcal/mol at the CASPT2 level. An IRC from the transition state TS_1−S_1 terminates at the 4-fold crossing point X−T_2/T_1/S_1/S_0 (toward the direction of further stretching the C−N bond). As addressed above, at X−T_2/T_1/S_1/S_0, the molecule is very likely to decay from the S_1 surface to the S_0 surface, producing the S_0 diazenyl biradicals (no minimum structure can be located on the S_0 surface). To investigate the energy profile for the second C−N bond cleavage, we performed a series of constrained optimizations at different C−N bond distances (all the other degrees of freedom were relaxed freely). The energy profiles associated

(45) The (4,4) active space consists of two radical orbitals (centered at the C and N atoms of the broken C−N bond) and σ, σ^* orbitals of the intact C−N bond.

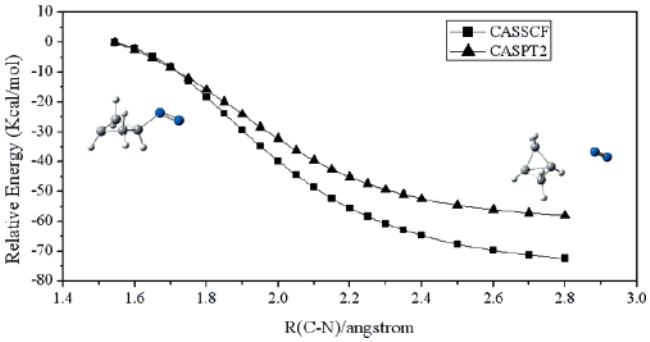

FIGURE 6. CASSCF and CASPT2 energy profiles of singlet diazenyl biradicals along the reaction coordinate of denitrogenation.

with this process are shown in Figure 6. One can see that at both CASSCF and CASPT2 levels the formation of the bicyclobutane **2** is strongly exoergic without involving any barrier. During this process, N_2 is displaced from backside by the carbon-centered radical to give the double inverted bicyclobutane exclusively. This S_H2 process can explain why excessive double inverted bicyclobutane **2** was observed during the photolysis of **1**. It should be mentioned that the decay pathway of the S_1 surface through ISC_1−T_2/S_1 (as discussed in the subsection **3.1**) might be competitive with this successive C−N cleavage pathway. But ISC_2−T_2/S_1 is not likely involved in this C−N breaking pathway because it is about 4 kcal/mol higher in energy than TS_1−S_1 (at the CASPT2 level), as seen from Table 1.

Let us turn our attention to the reaction path on the T_1 surface. The ZPE-corrected barrier for the first C−N bond cleavage (from M_1−T_1 to TS_3−T_1) is 6.6 kcal/mol at the CASPT2 level. An IRC calculation from TS_3−T_1 toward the forward direction (further stretching of the first C−N bond) showed that during the first C−N bond cleavage the second C−N bond would also break, producing a triplet 1,3-cyclobutadiyl and N_2 directly (without passing through the 4-fold crossing point). It should be mentioned that CI_2−T_2/T_1 is not likely involved in the pathway through TS_3−T_1 because it is about 11 kcal/mol higher in energy than TS_3−T_1 (at the CASPT2 level). The resulting triplet 1,3-cyclobutadiyl can be easily converted into the singlet 1,3-cyclobutadiyl, which can readily form stereorandomized bicyclobutane **2**, as demonstrated in previous works.[46−50]

3.3. Reaction Paths Involving the β C−C Bond Cleavage. 3.3.1. Reaction Path for Production of Hydrazone. Since some experimental evidence[34] showed that β C−C cleavage is likely to take place on the triplet excited surface, in the following we will focus on the PES of the lowest triplet state involving the β C−C bond cleavage. The active space (12,11) for describing this part of PES has been mentioned in Sec. II. At the CASSCF(12,11) level, the optimized structures of all stationary points and crossing points are shown in Figure 7, and their energies are listed in Table 2. In order to compare the energies of different stationary points on an equal footing, we

(46) Nguyen, K. A.; Gordon, M. S.; Boatz, J. A. *J. Am. Chem. Soc.* **1994**, *116*, 9241.
(47) Feller, D.; Davidson, E. R.; Borden, W. T. *J. Am. Chem. Soc.* **1982**, *104*, 1216.
(48) Gassman, P. G.; Greenlee, M. L.; Dixon, D. A.; Richtsmeier, S.; Gougoutas, J. Z. J. *J. Am. Chem. Soc.* **1983**, *105*, 5865.
(49) Budzelaar, P. H. M.; Kraka, E.; Cremer, D.; Schleyer, P. v. R. *J. Am. Chem. Soc.* **1986**, *108*, 561.
(50) Collins, S.; Dutler, R.; Rauk, A. *J. Am. Chem. Soc.* **1987**, *109*, 2564.

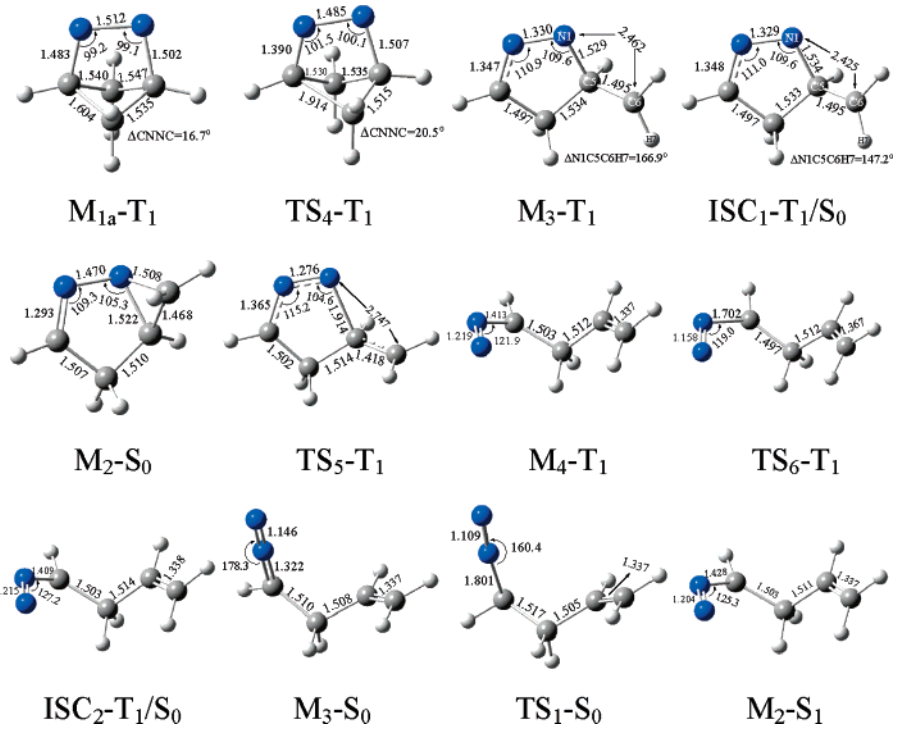

FIGURE 7. CASSCF(12,11)-optimized geometries of minima, transition states, and crossing points on the triplet excited-state PES involving the β C−C cleavage.

TABLE 2. Calculated CASSCF(12,11) and CASPT2 Energies of Stationary Points and Crossing Points on the Low-Lying States of 1

		relative energy[a] (kcal/mol)	
geometry	state	CASSCF	CASPT2
$M_{1a}-T_1$[b]	T_1	66.1	67.0 (65.1)
TS_4-T_1	T_1	72.2	74.7 (71.4)
M_3-T_1	T_1	19.1	40.2 (35.7)
	S_0	19.8	41.4
ISC_1-T_1/S_0[c]	T_1	19.6	40.5
	S_0	19.6	40.5
M_2-S_0	S_0	−22.5	−2.7 (−3.3)
TS_5-T_1	T_1	25.6	44.6 (38.9)
M_4-T_1	T_1	−1.2	28.3 (23.2)
	S_0	7.8	36.1
	S_1	15.2	40.4
TS_6-T_1	T_1	3.6	39.6 (32.7)
ISC_2-T_1/S_0[c]	T_1	1.9	29.1
	S_0	1.9	30.7
M_3-S_0	S_0	−34.1	1.3 (−2.5)
	S_1	39.8	64.1
	T_1	34.8	40.0
TS_1-S_0	S_0	−17.0	31.8 (26.1)
M_2-S_1[d]	S_1	14.8	40.0
	S_0	4.3	32.8
	T_1	−0.8	28.9

[a] The ZPE-corrected energies are shown in parentheses; the energy of the S_0 state at M_1-S_0 is set to zero. [b] The structures are optimized at the CASSCF(12,11) level. [c] State-averaged calculation with two states (T_1, S_0) being equally weighted. [d] State-averaged orbitals used.

reoptimized the structure of M_1-T_1 (described above) at the CASSCF(12,11) level, with the corresponding structure denoted as $M_{1a}-T_1$. The transition state corresponding to the β C−C cleavage is labeled as TS_4-T_1. The breaking C−C bond in TS_4-T_1 is 1.914 Å, significantly longer than that (1.604 Å) in the reactant $M_{1a}-T_1$. The barrier from $M_{1a}-T_1$ to TS_4-T_1 is calculated to be 6.3 kcal/mol at the CASPT2 level after ZPE corrections are added. After crossing TS_4-T_1, the system will reach a hydrazonyl biradical minimum M_3-T_1, as revealed by an IRC calculation. At the geometry of M_3-T_1, the S_0 state is only 1.2 kcal/mol above the T_1 state. In order to form a new C−N bond occurring in the product **4** (M_2-S_0), an ISC process from T_1 to S_0 is necessary. We have located a singlet−triplet crossing point, ISC_1-T_1/S_0, for this process. ISC_1-T_1/S_0 is just 0.5 kcal/mol above M_3-T_1 at the CASSCF(12,11) level (and 0.3 kcal/mol at the CASPT2 level). The main geometrical change from M_3-T_1 to ISC_1-T_1/S_0 is a rotation of the methylene group toward the N_1 atom (about 20°). Clearly, the rotation of the methylene group will increase the overlap between the two radical orbitals located at the N1 and the C6 atom, respectively, and thus stabilize the singlet hydrazonyl biradical so that the S_0 and T_1 surfaces can approach to each other. However, the calculated SOC at ISC_1-T_1/S_0 is quite small (0.80 cm^{-1}). Thus, although M_3-T_1 can easily reach ISC_1-T_1/S_0, the probability of the intersystem crossing from T_1 to S_0 at ISC_1-T_1/S_0 is expected to be not high. Thus, the triplet hydrazonyl biradical minimum M_3-T_1 would have enough time to rotate the methylene around the C5−C6 bond to scramble C6. As a consequence, the experimental fact[34] that the product **4** is stereorandomized at the C6 atom can be satisfactorily explained. On the other hand, once the triplet hydrazonyl biradical minimum transforms to the corresponding singlet species through ISC_1-T_1/S_0, we are concerned with the energy profile from ISC_1-T_1/S_0 to **4**. A relaxed PES scan along the C6−N1 bond distance (an approximate reaction coordinate) produces the energy profiles in Figure 8 (at both the CASSCF and CASPT2 levels). The results demonstrate that the production of hydrazone (**4**) from the singlet hydrazonyl biradical is a spontaneous process on the S_0 surface.

3.3.2. Reaction Paths for Production of the Intermediate Species 2-Allyldiazomethane and Allylmethylene. As discussed above, M_3-T_1 may convert into M_2-S_0 through ISC_1-

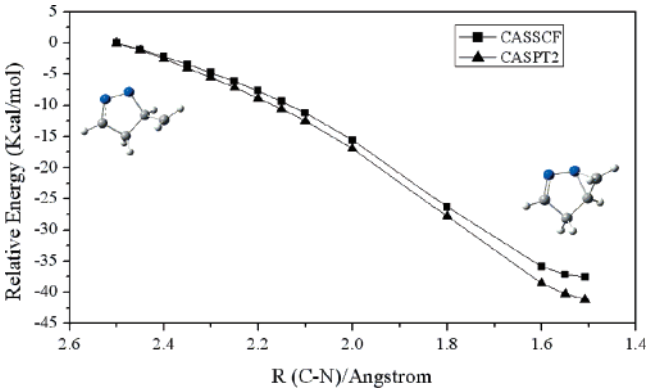

FIGURE 8. CASSCF and CASPT2 energy profiles from the singlet hydrazonyl biradical to hydrazone along the C−N bond distance.

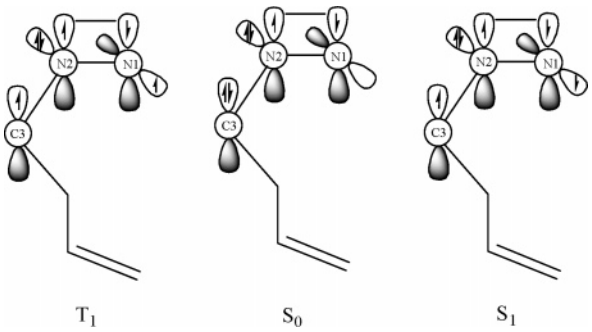

FIGURE 9. Electron configurations of the T_1, S_0, and S_1 states near the geometry of M_4-T_1.

T_1/S_0. On the other hand, it may break the C5−N1 bond to form 2-allyldiazomethane **5** (M_4-T_1) through the transition state TS_5-T_1. As shown in Figure 7, the breaking C−N bond in TS_5-T_1 is 1.914 Å. The barrier for this C−N bond breaking is 3.2 kcal/mol at the CASPT2 level (with ZPE corrections). With such a low barrier, this C−N breaking pathway could compete with the ISC process through ISC_1-T_1/S_0, which is energetically very favorable but with a small SOC. Also, we have tried to optimize a transition state involving a concerted cleavage of both C−C and C−N bonds, which was suggested in the literature.[34] But our numerous attempts all failed. Thus, our calculations demonstrated that the formation of 2-allyldiazomethane **5** occurs by a stepwise mechanism (first C−C and then C−N cleavage).

At the geometry of M_4-T_1, the energies of three states T_1, S_0, and S_1 are quite close with the energy ordering $T_1 < S_0 < S_1$. The electron configurations of these three states within the active space are schematically shown in Figure 9. Since one p orbital of the C3 atom is doubly occupied in the S_0 state but singly occupied in the T_1 and S_1 states, the singlet carbene can be generated directly from the S_0 state by breaking the second C−N bond. Similarly, the triplet carbene can be generated directly from the T_1 state, as will be shown below.

By breaking the second C−N bond, M_4-T_1 can produce N_2 and the terminal triplet carbene (allylmethylene) through a transition state TS_6-T_1, whose barrier height is 9.5 kcal/mol at the CASPT2 level (with ZPE corrections). M_4-T_1 may also convert into a singlet minimum, 2-allyldiazomethane (M_3-S_0), through ISC_2-T_1/S_0, which is only 0.8 kcal/mol above M_4-T_1 at the CASPT2 level. The N═N−C angle in ISC_2-T_1/S_0 is about 5° larger than that in M_4-T_1. Thus, one can see that a slight expansion of the N═N−C angle would allow M_4-T_1 to reach ISC_2-T_1/S_0 (little energy is required for this process).

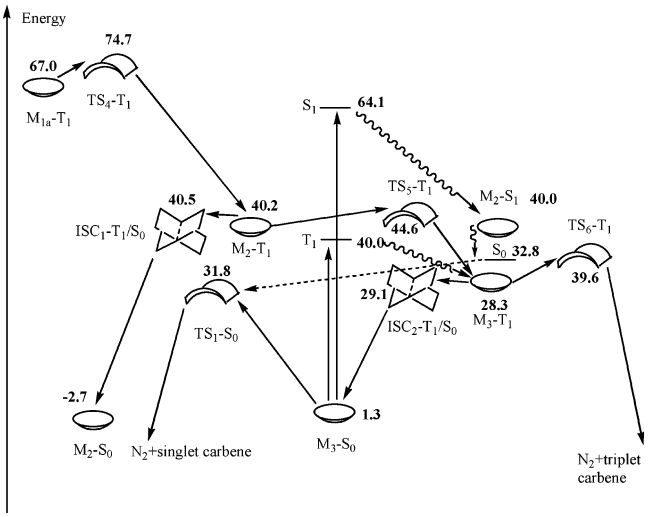

FIGURE 10. Summary of processes involving the C−C cleavage.

Since the SOC value at ISC_2-T_1/S_0 is quite large (24.1 cm^{-1}), the intersystem crossing at ISC_2-T_1/S_0 should be quite efficient. Once the system transforms to the S_0 surface at ISC_2-T_1/S_0, the production of M_3-S_0 becomes spontaneous (an exoergic process). This result is in accord with the fact that diazoalkene **5** (M_3-S_0) was generated during the photolysis of **1**.[34]

M_3-S_0 can also break the second C−N bond to form N_2 and a singlet allylmethylene, through a transition state TS_1-S_0. The ZPE-corrected barrier for this process on the S_0 surface is 28.6 kcal/mol at the CASPT2 level. Such a high barrier could prohibit the generation of the singlet allylmethylene on the S_0 surface. On the S_1 surface we located a minimum M_2-S_1 near the geometry of M_4-T_1 at the CASSCF(12,11) level. At the geometry of M_2-S_1 the S_0 state lies just 7.2 kcal/mol below the S_1 state at the CASPT2 level. Previous theoretical study on diazomethane had shown that the S_1 state of diazomethane can easily transfer to the S_0 state by the internal conversion and then produce $^1CH_2$ plus N_2.[51] Since M_3-S_0 is structurally similar to diazomethane, one would expect that the photochemical denitrogenation behavior of M_3-S_0 is also similar to that of diazomethane. Thus, the internal conversion from the S_1 state to the S_0 state should also be relatively efficient for M_3-S_0, once it is excited to the S_1 surface. As a result, it is possible that M_3-S_0 can produce N_2 and the terminal singlet carbene upon direct irradiation. For clarity, we have shown all stationary points and crossing points involving the C−C bond cleavage in Figure 10.

3.3.3. Reaction Paths for Production of Butadiene and Bicyclobutane via Allylmethylene. For allylmethylene, our CASSCF(6,6)[54] calculations led to a minimum structure M_4-S_0 on the singlet state surface and another minimum M_5-T_1 on the triplet surface, the latter being 8.9 kcal/mol below the former. For these two species and other species involving in the deactivation paths of these two species, their structures are displayed in Figure 11, with their energies listed in Tables 3 and 4. It is well-known that these two species may transform

(51) Yamamoto, N.; Bermardi, F.; Bottoni, A.; Olivucci, M.; Robb, M. A.; Wilsey, S. *J. Am. Chem. Soc.* **1994**, *116*, 2064.
(52) (a) Skell, P. S.; Woodworth, R. C. *J. Am. Chem. Soc.* **1956**, *78*, 4496.
(53) Skell, P. S.; Woodworth, R. C. *J. Am. Chem. Soc.* **1959**, *81*, 3383.
(54) The (6,6) active space consists of two carbene orbitals, π, π^* of the C═C bond and the σ, σ^* orbitals of the C−H bond to be broken.

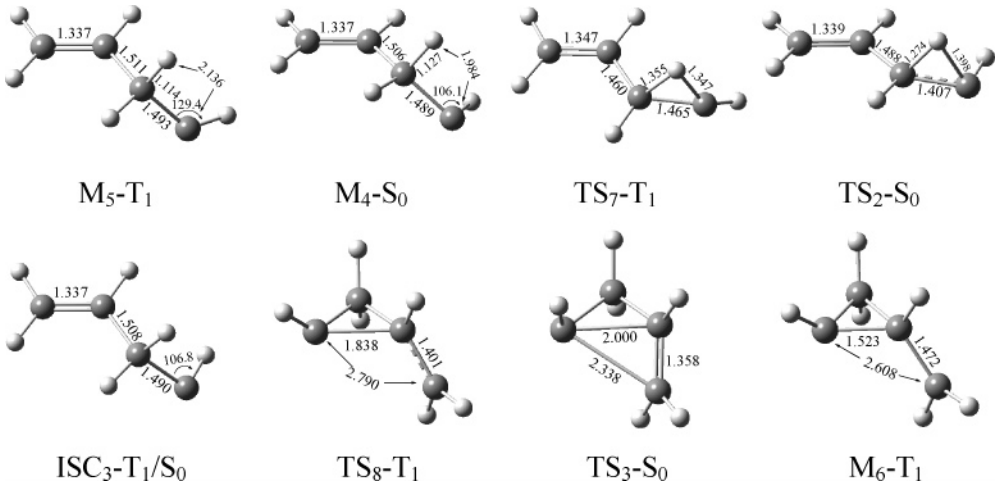

FIGURE 11. CASSCF(6,6)- and (4,4)-optimized geometries of minima, transition states, and crossing points related to the terminal carbene species.

TABLE 3. Calculated CASSCF(6,6) and CASPT2 Energies of Stationary Points and Crossing Points for the Triplet and Singlet Carbene

		relative energy[a] (kcal/mol)	
geometry	state	CASSCF	CASPT2
M_5-T_1	T_1	0.0	0.0
M_4-S_0	S_0	6.8	9.2 (8.9)
TS_7-T_1	T_1	52.6	40.9 (37.1)
TS_2-S_0	S_0	12.7	7.3 (6.0)

[a] The ZPE-corrected energies are shown in parentheses. The energy of the T_1 state at M_5-T_1 is set to zero.

TABLE 4. Calculated CASSCF(4,4) and CASPT2 Energies of Stationary Points and Crossing Points for the Triplet and Singlet Carbene

		relative energy[b] (kcal/mol)	
geometry	state	CASSCF	CASPT2
M_5-T_1[a]	T_1	0.0	0.0
M_4-S_0[a]	S_0	6.6	9.0 (8.7)
ISC_3-T_1/S_0[c]	T_1	12.6	10.1
	S_0	12.6	10.5
TS_8-T_1	T_1	25.7	13.2 (12.4)
TS_3-S_0	S_0	12.0	0.2 (1.3)
M_6-T_1	T_1	18.1	4.1 (4.1)

[a] The structures are optimized at the CASSCF(4,4) level; the energy of the T_1 state at M_5-T_1 is set to zero. [b] The ZPE-corrected energies included in the parentheses. [c] State-averaged calculation with two states (T_1, S_0) being equally weighted.

into butadiene by 1,2-hydrogen shift or bicyclobutane through the addition of the carbene center to the C═C double bond.[52,53]

For the 1,2-hydrogen shift pathway, we have obtained the transition states TS_2-S_0 and TS_7-T_1 on the singlet and triplet surfaces, respectively. The calculated barriers for this process are 5.9 kcal/mol on the singlet surface, but 52.6 kcal/mol on the triplet surface at the CASSCF(6,6) level. At the CASPT2 level, the barrier on the singlet state disappears, but the barrier on the triplet surface is still 37.1 kcal/mol. Thus, one can conclude from our calculations that the formation of butadiene would take place easily only on the singlet surface.

For the carbene addition pathway, we have located two transition states, TS_3-S_0 and TS_8-T_1, on the sinlget and triplet surfaces, respectively, at the CASSCF(4,4)[55] level. To estimate the relative energies of some species on an equal footing, the structures of M_4-S_0 and M_5-T_1 (discussed above) are reoptimized at the CASSCF(4,4) level, and their energies are listed in Table 4 for comparison. As seen from Table 4, at the CASPT2 level the carbene addition to the C═C double bond is a barrierless process on the singlet surface (via TS_3-S_0). But on the triplet surface, the barrier from M_5-T_1 to M_6-T_1 through TS_8-T_1 is 12.4 kcal/mol. The surface crossing point ISC_3-T_1/S_0 between the T_1 and S_0 states was located to lie about 10 kcal/mol above M_5-T_1 at the CASPT2 level. It should be mentioned that the triplet biradical minimum M_6-T_1 may decay to the S_0 surface through an ISC process and then undergo a C−C coupling process to form the final product bicyclobutane. However, a comparison of the results described above suggests that the carbene addition to the C═C double bond is preferred to occur on the S_0 surface.

3.4. Brief Comparison of the Studied System with DBO and DBH in the Photochemical Behavior. According to our results in this work, the photochemical behavior of **1** differs from that of DBO or DBH in several aspects. First, in the Franck−Condon region, **1** has a symmetric minimum structure on the S_1 ($n-\pi^*$) surface, whereas DBO or DBH has a symmetric transition state, with the transition vector being the twisting of the C−N═N−C bridge in DBO[33] or the bending of two NNC angles in DBH.[19] This result can be attributed to the relatively higher ring strain in **1** than that in DBO or DBH. Second, near the Franck−Condon region the intersystem crossing from the S_1 surface to the T_2 ($\pi-\pi^*$) surface is predicted to be favorable in **1** but inefficient[33] in DBO (DBH has a similar behavior as **1**[19]). Third, on the S_1 surface the calculated barrier for α C−N bond cleavage is about 5 kcal/mol in **1** and DBH,[20] which is significantly lower than that in DBO.[33] On the T_1 surface the corresponding barrier for α C−N bond cleavage is about 7 kcal/mol in **1**, 9 kcal/mol in DBO,[33] 16 kcal/mol in DBH.[19] The lower barriers for α C−N bond cleavage and an efficient ISC process (near the Franck−Condon region) make **1** to denitrogenate efficiently, unlike DBO. Finally, on the triplet excited-state the barrier for the β C−C bond cleavage is calculated to be about 6 kcal/mol in **1**, being much lower than

(55) The (4,4) active space consists of two carbene orbitals, π, π^* of the C═C bond .

that (24 kcal/mol) in DBH[19] (this route has not been theoretically investigated for DBO). This relatively low barrier for the β C−C bond cleavage accounts well for the experimental fact that the photoproduct hydrazone was observed in **1** (but not in DBH and DBO).

4. Conclusions

In this paper, we have used the CASPT2//CASSCF method to study the mechanism of the photolysis of 2,3-diazabicyclo-[2.1.1]hex-2-ene **1**. By exploring its low-lying excited-state potential energy surfaces near the Franck−Condon region, and the C−N, C−C bond cleavage regions, we have been able to present a detailed picture on the complex photophysical and photochemical processes of this compound under direct irradiation and triplet-sensitized irradiation. The calculated singlet 0−0 excitation energy and vertical emission energy from the S_1 state agree well with the experimental data. For the formation of three photoproducts, bicyclobutane, butadiene, and 1,2-diazabicyclo-[3.1.0]hex-2-ene, we can draw the following conclusions from our calculations. (1) On direct irradiation, first a C−N bond in the studied system is likely to break on the S_1 surface, producing the diazenyl biradical. Then, a concerted C−N cleavage (another C−N bond) and C−C coupling process (S_H2 pathway) would yield the photoproduct bicyclobutane. (2) Another deactivation path for the S_1 state is to transfer to the triplet state through an efficient ISC process. This would explain why butadiene and 1,2-diazabicyclo[3.1.0]hex-2-ene can be produced on direct irradiation. (3) On the T_1 surface, the C−C bond cleavage is easy to occur, forming the triplet hydrazonyl biradical. This biradical intermediate could cross to the S_0 surface to initiate a barrierless C−N bond-making process, which will result in the photoproduct 1,2-diazabicyclo[3.1.0]hex-2-ene. (4) The triplet hydrazonyl biradical could also break one C−N bond to form the intermediate 2-allyl-diazomethane. This intermediate then breaks the second C−N bond to generate a terminal carbene species, which could finally convert into two photoproducts, bicyclobutane and butadiene.

Acknowledgment. This work was supported by the National Basic Research Program (Grant No. 2004CB719901), the National Natural Science Foundation of China (Grant Nos. 20373022 and 20233020), the Chinese Ministry of Education (Grant No. NCET-04-0450), and the Fok Ying Tong Education Foundation (Grant No. 91014). We also thank the Virtual Laboratory of Computational Chemistry, Computer Network Information Center, Chinese Academy of Science, for providing computational resources.

Supporting Information Available: Calculated absolute energies, Cartesian coordinates of all stationary points and surface intersections, and information on the frequency and transition vectors of transition states and the corresponding branching space of conical intersections. This material is available free of charge via the Internet at http://pubs.acs.org.

JO0611622